energies

MDPI

Article

Experimental Study on the Factors Influencing the Heat Transfer Coefficient of Vertical Tube Indirect Evaporative Coolers

Tiezhu Sun *, Guangyu Tian, Peixuan Li, Wenkang Li and Huan Sun

School of Urban Planning and Municipal Engineering, Xi'an Polytechnic University, Xi'an 710048, China; 18326811709@163.com (G.T.); 19991832069@163.com (P.L.); 15529378917@163.com (W.L.); 211421055@stu.xpu.edu.cn (H.S.)

* Correspondence: suntiezhu66@163.com; Tel.: +86-18991921966

Abstract

This study looks into the parameters that affect the heat transfer coefficient (h_2) on the wet surfaces of vertical tube indirect evaporative coolers (VTIEC). An experimental platform was used to investigate the impact of secondary-to-primary airflow ratios (AFR) and spray water density on the HTC. The findings show that raising the primary air temperature drop, expanding the outside dry-bulb and wet-bulb temperature differences, and decreasing the air-to-water ratio improve heat transmission. The HTC of the wet sides ranged from 34.79 to 924.5 W/(m^2·°C) throughout testing. To achieve optimal performance, aim for a spray water density of 2.07 to 3.46 m^3/(m^2·h), an AFR of 0.5 to 0.6, and a primary air temperature drop of at least 6 °C. These factors help keep the h_2 above 350 W/(m^2·°C).

Keywords: vertical tube indirect evaporative cooler; heat transfer coefficient; airflow ratio; water flow rate; water spraying density

1. Introduction

As society evolves, energy and environmental pollution problems worsen. Because air conditioning consumes the bulk of energy in buildings, researching the development of clean and efficient renewable energy technologies is one of the primary strategies to achieve the "dual-carbon" goal. In the context of the worldwide "dual-carbon" strategy, evaporative cooling is an energy-saving technology with a wide range of applications. It is currently widely employed in various industries and has produced good results [1]. The supply air's high humidity limits direct evaporative cooling (DEC) [2–4]. Indirect evaporative cooling (IEC) overcomes this difficulty by providing effective cooling through indirect heat exchange mechanisms. IEC differs from standard DEC systems in its capacity to accomplish iso-humidity cooling. This is accomplished by an ingenious design that employs an indirect heat exchange method between the supply and return air. The fundamental distinction is that the IEC uses a drench to directly chill the return air before indirectly cooling the source air [5]. As a result, this indirect heat exchange mechanism considerably expands the range of evaporative cooling applications.

In recent years, scholars have conducted numerous studies to optimize the structure of IEC systems and discovered that the IEC system can replace traditional cooling systems based on compression cycles in buildings and other applications [6–8]. The IEC system can be classified according to its shape. IEC systems are classified by shape into horizontal tubes, plate fins, vertical tubes, dew points, heat pipes, and so forth. The tube type is

check for updates

Academic Editor: Artur Blaszczuk

Received: 23 September 2025
Revised: 12 November 2025
Accepted: 12 November 2025
Published: 13 November 2025

Citation: Sun, T.; Tian, G.; Li, P.; Li, W.; Sun, H. Experimental Study on the Factors Influencing the Heat Transfer Coefficient of Vertical Tube Indirect Evaporative Coolers. *Energies* **2025**, *18*, 5967. https://doi.org/10.3390/en18225967

Copyright: © 2025 by the authors. Licensee MDPI, Basel, Switzerland. This article is an open access article distributed under the terms and conditions of the Creative Commons Attribution (CC BY) license (https://creativecommons.org/licenses/by/4.0/).

the most commonly utilized type of heat exchanger. This study's focus, the vertical tube-type IEC (VTIEC), offers a structural compromise: Compared to the traditional plate-fin and horizontal tube types, the vertical tube indirect evaporative cooler (VTIEC) has the advantages of not clogging easily, having a small footprint, being widely applicable, being cost-effective, and being widely used in actual projects [9].

IEC systems offer considerable benefits in terms of energy savings and applications, prompting extensive study into investigating and improving IEC system performance. Current research has mostly focused on optimizing structural materials, increasing heat transfer efficiency, improving spray devices, and optimizing operating systems [10–13]. Investigating the parameters that influence the performance of IEC systems can result in targeted improvements in cooling efficiency. Sohani [14] developed a two-stage direct-indirect evaporative cooler and investigated the impacts of changing effective parameters on various system performance criteria while conducting economic analysis research. Sun [15] et al. adjusted the input parameters for a single-tube model of a porous ceramic tube IEC, resulting in better product performance. Sun [16] investigated the convective heat transfer coefficient of TIEC units at outdoor dry bulb temperatures of 16–18 °C and summarized the major elements influencing IEC convective heat transfer. Yuan [17] investigated the effects of flow and area distribution on the performance optimization of IEC systems using energy analysis and thermal resistance methods and found that the thermal resistance decreased to a minimum when the cooling capacity reached its maximum value, but the energy efficiency did not reach its maximum. Thus, rather than energy efficiency, thermal resistance is used to characterize the heat transfer performance of evaporative cooling systems.

The heat transfer coefficient (HTC) is the reciprocal of thermal resistance, and the overall HTC of IEC systems can be used to determine the system's heat transfer performance directly. Theoretically, increasing the HTC allows for the same heat transfer effect to be achieved with a smaller heat transfer surface, lowering the cost of heat exchanger production. For VTIEC systems, the overall HTC should be a combination of wall conduction, heat transfer over the tube bundle in the dry channel, and wet-side h_2. The first two heat transfer processes are easier and more correctly estimated with criteria correlations. However, the heat transfer process in the wet channel is a more complex two-phase flow than simple air-air heat transfer. It is a complex procedure because the channel contains both water and air, as well as a 'water film' phenomenon. The presence of h_2 on wet surfaces complicates the total heat transfer process of VTIECs, making it difficult to precisely measure using theoretical research. This intricacy in estimating the h_2 of wet surfaces presents a significant challenge. This issue is also widespread in theoretical estimates of IEC systems.

Researchers often conduct experimental testing or numerical simulations to investigate HTC in IEC systems. Jamil reviewed and compared the findings of numerous investigations on HTC in IEC systems, developing a correlation between HTC systems designed and scaled up on an industrial scale. The correlation was created for industrial-scale designs and scaled-up systems. Incorporating the effect of the system's evaporative potential into the HTC calculations significantly enhances their accuracy. In evaporative cooling system research, "thermal resistance/heat transfer coefficient" more directly describes the heat transfer mechanism (boundary layer, phase change, etc.), whereas "energy efficiency" usually refers to the system energy input/output and equipment efficiency. Therefore, this study concentrated on dry channel h_1 and did not account for the effect of external wet bulb temperature. As a result, these correlation findings are limited to environmental parameter requirements. To calculate the h_2 of wet sides in IEC systems, researchers often establish empirical formulas based on extensive experiments, fitting the HTC of various models using dimensionless parameters such as the Nusselt number (Nu), Reynolds number (Re),

and Prandtl number (Pr). For heat transfer on the wet side of the IEC system, Ranz's equation (1952) is one of the most reliable correlation equations for calculating heat transfer from water droplets. However, because the IEC system is not completely full of water, this formula is incorrect.

Hasan [18] created an analytical model for a heat exchanger to accomplish sub-humid bulb cooling using a modified ε-NTU approach. Rajski [19] studied the impact of various operating parameters on the performance of an indirect evaporative cooler based on gravity-assisted heat pipes and identified the most efficient operating conditions for the system. Wan [20] created a computational fluid dynamics (CFD) model to study heat and mass transmission in IEC systems that include condensation phenomena. The impacts of nine parameters on the heat and mass transfer process in IEC systems were investigated using orthogonal experiments, and empirical correlations between the average HTC and mass transfer coefficients were found. Lin [21] investigated the heat and mass transfer coefficients of dew-point evaporative coolers using theoretical approaches and CFD simulations. The study revealed the primary contributing factors that affect heat and mass transfer effects, as well as the parameter ranges for each. These findings show that naturally occurring boundary conditions have better heat transfer properties than generally accepted boundary conditions. As a result, the numbers determined experimentally outperformed those calculated theoretically.

In summary, current research on the HTC in IEC systems is primarily based on empirical calculations and CFD simulations. However, both have limitations: empirical formulas have excessively large errors, and CFD simulations frequently fail to produce real-world outcomes. Accurately determining the overall HTC in IEC systems is a difficult undertaking due to the numerous parameters impacting the HTC of wet sides. And the specific impact of each element on this coefficient has not been thoroughly investigated. To bridge this gap, experimental research provides a more realistic method for assessing the performance of IEC systems.

As a result, this research focuses on testing the performance of VTIECs under various operating situations using experimental methods. The study sought to find HTC on the wet surfaces of VTIECs, as well as to establish the factors that influence them and their impacts. The findings provide a solid foundation for improving the performance of such systems while also providing significant insights into the heat transfer performance of other types of IECs.

2. Experimental Design

2.1. Theoretical Model

The VTIEC has a unique structure when compared to typical horizontal tubes and plate-fin IECs. Primary air moves along the outside of the heat exchanger tube, while secondary air and circulating water move inside. A pump distributes the flowing water from the top of the unit, which descends as a film over the inner tube surface. Secondary air enters from below, exchanges heat with the water film, and cools the primary air in the dry channel. The primary air flows vertically over the heat exchanger surface in the dry channel, while the fan discharges secondary air from the top to generate the wet channel. This configuration enables humid cooling [9]. Water layer evaporation and convection at the gas–liquid interface are what propel a VTIEC's wet-side heat and mass transfer. Convection and conduction work together to control the sensible heat flux, while evaporation uses latent heat transfer to accomplish bulk cooling. The interfacial enthalpy difference drives this coupled process, and the water film thickness, air velocity, and wall temperature regulate its mass transfer efficiency. These factors, in turn, control the liquid-side thermal resistance, boundary layer formation, and the strength of the driving force for evaporation.

Secondly, the wet-side heat transfer process involves coupled heat and mass transfer between air and a water film, exhibiting significant unsteady and nonlinear characteristics. The evaporation process itself is unsteady, influenced by air velocity fluctuations, variations in the water film supply, and the dynamic wall temperature distribution, resulting in significant temporal and spatial variations in the local evaporation rate. Latent heat release is tightly coupled with gas-phase diffusion processes, forming a coupled heat and mass transfer boundary layer, making it difficult to obtain an analytical solution to the enthalpy equation. Existing enthalpy models or empirical correlations often assume steady-state behavior and use average enthalpy differences to characterize heat and mass fluxes. These models fail to fully account for the effects of film thickness variations and local evaporation dynamics on the heat transfer process, making it difficult to fully characterize the wet-side heat transfer mechanism. To balance computational efficiency and physical plausibility, this study calibrated a simplified theoretical model using experimentally measured parameters. Specifically, when constructing the energy balance equation, the dominant terms (sensible heat exchange and latent heat evaporation) were retained, and the equivalent heat transfer coefficient was determined based on measured temperature and humidity data [22].

Figure 1 depicts the structure and heat exchange principles of a VTIEC. The primary air system, secondary air system, circulating water system, and vertical arrangement of heat exchange tubes with specific heat exchange performance are the key components [16]. Figure 2 depicts the heat and mass transport mechanisms within a single tube of the VTIEC. The system has three types of fluids: primary air, circulating water (water film and droplets in the tube), and secondary air.

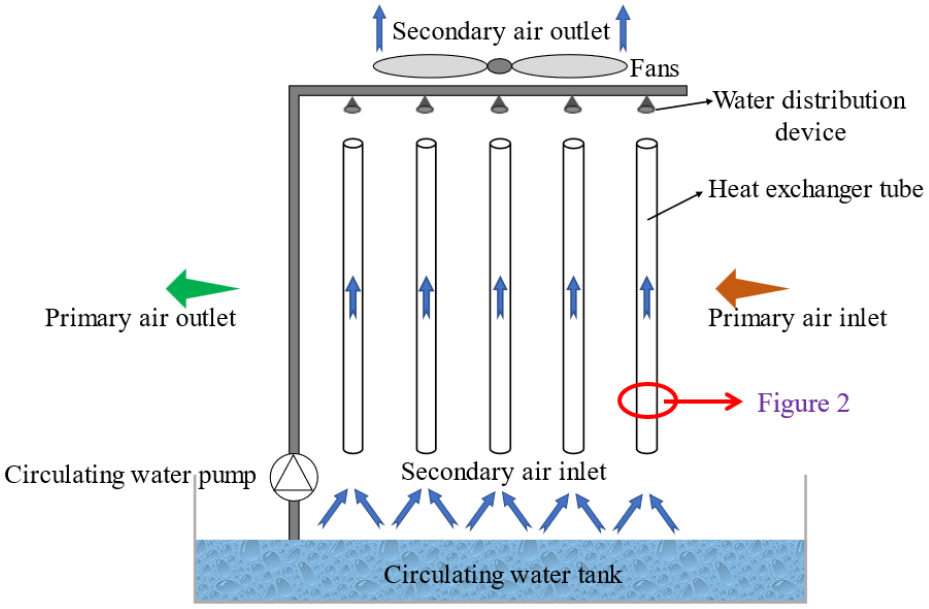


Figure 1. Schematic diagram of a VTIEC.

The h_1 of the dry channel is proportional to the convective heat transfer of the outer swept tube bundle, which can be computed using the heat transfer principle. For the convective heat transfer of the outer swept tube bundle, the corresponding criterion correlation formula can be selected to calculate the h_1 of the dry channel, and these correlation formulas have been validated by a large number of data, ensuring the accuracy of the results. Heat transfer in the wet channel is a complex two-phase flow characterized by the "water film" phenomenon. Maintaining a uniform water film and a strict countercurrent configuration in a small diameter pipe (<½ inch) is inherently difficult. However, by designing the vertical pipe, the overall air and water film flows in countercurrent. This arrangement utilizes

gravity to assist drainage, which is more conducive to reducing flow unevenness and water accumulation problems compared to horizontal pipe bundles [23]. This work estimates the air-side benchmark heat transfer coefficient using the cross-swept tube bundle correlation established by Zhukauskas [1] as the calculation base. This correlation has been widely utilized in engineering estimates of cross-tube heat transfer and has been validated for similar geometries and Reynolds values. This is the formula shown in Equation (1), with the Nusselt number (*Nu*) obtained from Equation (2). However, with IECs, the fraction of two-phase flow inside the wet sides varies, making it impossible to quantify the integrated HTC. The integrated thermal conductivity (HTC) cannot be reliably determined by simple averaging or analytical integration because of the unequal distribution of local heat flow and wall temperature variations during heat transfer. The interfacial evaporation rate is nonlinearly influenced by local temperature, humidity, and flow rate, resulting in instability phenomena such as local dry spots and droplet entrainment in the system as it moves at high speeds. Under conditions of unstable or two-phase heat transfer, this issue is most noticeable [24]. To confirm the calculation's physical plausibility, this study used an experimental fitting method to get the average HTC. This approach circumvents the significant mistakes that result from ignoring the connection of phase change latent heat, the variable of wet film thickness, and the uncertainty of boundary conditions [25,26].

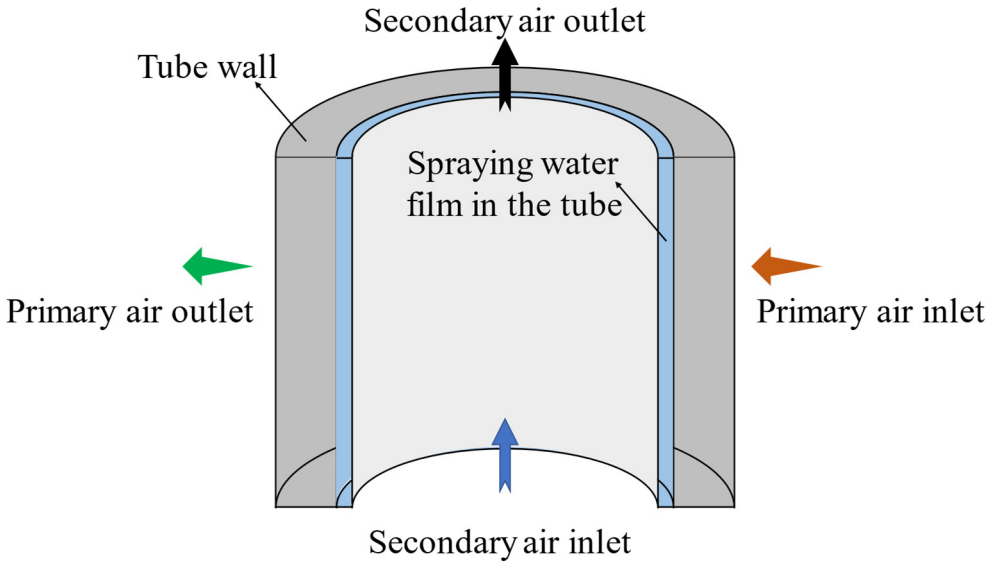


Figure 2. Schematic diagram of heat and mass transfer in the tube.

$$Nu = C \cdot Re^{y} Pr^{0.36} \cdot \left(\frac{\mathrm{Pr}}{\mathrm{Pr}_s}\right) \quad (1)$$

where *Re* and the tube bundle's geometric characteristics (S_1, S_2) define *C* and y. S_1 and S_2 are the horizontal and vertical spacing of the tube bundles. This is the formula's central idea, illustrating how the arrangement directly affects heat transfer. Typically, n is 0.36. $\mathrm{Pr}/\mathrm{Pr}_s$ can be set to 1. Pr_s is the Prandtl number at the tube surface.

$$Nu = \frac{h \cdot d}{\lambda} \quad (2)$$

The h_1 of the dry channel is proportional to the convective heat transfer of the outer swept. To ease the computation and study of the mathematical model, the following assumptions are made about it: (1) Air and water are assumed to be constant properties, and the fluid is treated as incompressible. (2) Radiation heat loss from the core to the surroundings is ignored (radiation heat transmission within the parameter range addressed

in this research accounts for less than 5% of overall heat transfer). (3) Thermal resistance due to dirt inside the core is ignored. (4) The temperature of the water film inside the channel is assumed to be constant. We also understand that any empirical correlation has intrinsic prediction errors as a result of measurement dispersion, differences in experimental conditions, and fitting simplification. After reviewing the literature on tube bundle heat transfer and conducting uncertainty analysis, empirical correlations in engineering applications often have a prediction error of ±15% [25].

IEC design calculations are frequently studied using the logarithmic mean temperature difference (LMTD) approach [9]. This calculating approach is straightforward; however, in coupled heat and mass transfer processes, both heat exchange and mass exchange occur at the same time, which violates the basic assumptions of adiabatic heat transfer in heat transfer theory. To address the issue of average heat transfer temperature differences and average mass transfer humidity differences becoming meaningless in some circumstances, the logarithmic mean enthalpy difference approach can be used for processing [27]. Therefore, this paper employs an enthalpy model for theoretical analysis on the wet side. By incorporating sensible and latent heat into the energy conservation equation and using specific enthalpy as a state variable, this model avoids the difficulty of separating the dry and wet zones in phase change heat transfer. Its spatial distribution is difficult to determine directly within a narrow 10 mm flow channel. To overcome this problem, this study used a macroscopic thermodynamic equilibrium technique. The logarithmic mean enthalpy difference (Δi_m) driving heat and mass movement was estimated by carefully measuring the dry-bulb and wet-bulb temperatures of the air at the channel's input and outflow. This method successfully describes the net driving force throughout the channel using boundary state parameters, avoiding the technological limitations of microscale measurements while maintaining the physical rigor of coupled heat and mass transfer analysis. This enthalpy difference approach accurately captures the combined effects of heat and mass transport and has been used in studies on wet film heat transfer and indirect evaporative cooling [24].

The whole heat transfer (including sensible and latent heat) on the heat exchanger's air side can be described as enthalpy-driven heat transfer, that is, using an equivalent enthalpy model. The equivalent enthalpy model rigorously proves the wide applicability and theoretical validity of the logarithmic mean enthalpy difference approach in heat exchangers with mass transfer processes. This method overcomes the common linearization assumptions in traditional numerical integration, resulting in a reliable design tool equivalent to the classical logarithmic mean temperature difference method under no mass transfer conditions. It is especially suitable for analyzing two-fluid coupled heat and mass transfer processes under known boundary conditions [28]. Equation (3) is the fundamental equation for heat exchanger calculation. To assure the correctness of the experimental results, the HTC of the dry channel is calculated using the heat transfer principle, and the overall HTC is then utilized to determine the h_2 of the wet sides:

$$K_{eq} \mathrm{A} \Delta i_m = \Phi \tag{3}$$

Δi_m represents the log-mean enthalpy difference. Using enthalpy as a unifying driving force, we can capture both sensible and latent heat transport. Figure 3 depicts the heat and mass transfer mathematical model of the vertical thin-walled evaporator internal channel. In order to simulate heat transmission between two fluids across a partition wall, this schematic illustration builds a thermal resistance network model. The physical structure is depicted in Figure 3a, together with the wall temperature, convection heat transfer coefficient, wall thickness, and fluid temperatures on both sides. Figure 3b illustrates how this is abstracted into a series of thermal resistance circuits. The link between temperature distribution and thermal resistance along the heat transfer path is intuitively represented by

the total thermal resistance, which is made up of the conductive resistance of the wall and the convective resistance on both sides, which is analyzed from the outside. The convective HTC between the primary air and the wall surface is denoted by h_1, whereas the wet-side HTC of the two-phase flow of secondary air and circulating water is represented by h_2. δ_1 represents the wall thickness, while δ_2 represents the thickness of the water film. K_{eq} is the equivalent total mass transfer coefficient based on the enthalpy difference. The degradation of liquid film distribution (loss of effective area) produced by the narrow tube curvature, along with the greater effect of the staggered arrangement on gas-side mass transfer, is expected to be roughly offset. As a result, the K_{eq} obtained from the flat plate model is still valid under the parameters of this investigation. A is the total heat transfer area, and c_p is the specific heat capacity of air at constant pressure. The total HTC of the heat exchanger is computed as follows:

$$K_{eq} = \frac{1}{\left(\frac{1}{h_1} + \frac{\delta_1}{\lambda_1} + \frac{1}{h_2}\right)c_p} = \frac{\Phi}{A\Delta i_m} \tag{4}$$

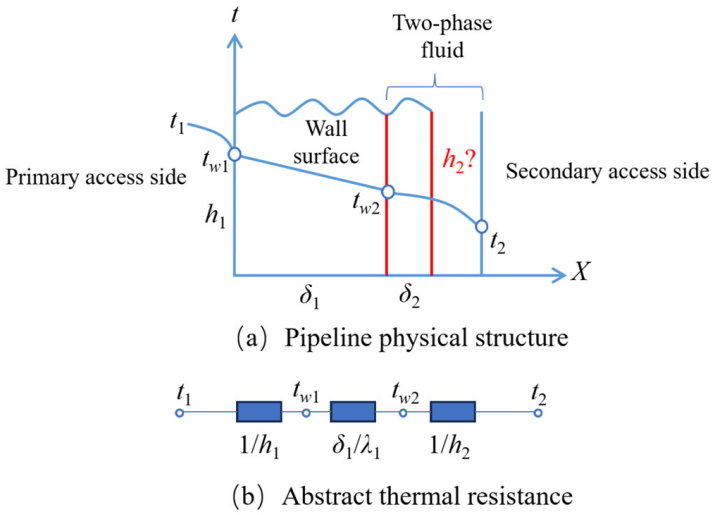


Figure 3. Schematic diagram of the heat transfer resistance.

In Figure 3, t_1 indicates the primary air temperature, and t_2 represents the secondary air temperature. In Equation (4), except for the HTC of wet sides h_2, which is difficult to find a correct value for, all other parameters may be evaluated, or the criteria equation can be used to find a more accurate value. As a result, inverting the value of h_2 in the equation yields a more accurate result.

Equations (5)–(7) determine the log mean enthalpy difference (Δi_m) in heat transfer using the enthalpy values of primary and saturated air at the water film surface. $\Delta i'$ represents the difference between the inlet air enthalpy (i_{g1}) and the water film enthalpy (i_f). The "potential energy" that propels the movement of mass and heat (like water vapor) from the air to the water film (or vice versa) at the intake increases with the size of this differential. $\Delta i''$ represents the difference between the outlet air enthalpy (i'_{g1}) and the water film enthalpy (i_f).

$$\Delta i' = i_{g1} - i_f \tag{5}$$

$$\Delta i'' = i'_{g1} - i_f \tag{6}$$

$$\Delta i_m = \frac{(\Delta i' - \Delta i'')}{\ln \frac{\Delta i'}{\Delta i''}} \tag{7}$$

Total heat transfer Φ (W):

$$\Phi = \rho_1 Q_1 C_{p1}(t_{g1} - t'_{g1}) \tag{8}$$

The heat balance equation for primary air-to-wall heat transfer is as follows:

$$m_1 C_{p1}(t_{g1} - t'_{g1}) = \pi d L h_1(\overline{t_{g1}} - T_W) \tag{9}$$

Average temperature of primary air (°C):

$$\overline{t_{g1}} = t_f + \Delta t_m \tag{10}$$

The log mean temperature difference (°C) can be calculated using Equations (11) to (13):

$$\Delta t' = t_{g1} - t_f \tag{11}$$

$$\Delta t'' = t'_{g1} - t_f \tag{12}$$

$$\Delta t_m = \frac{(\Delta t' - \Delta t'')}{\ln \frac{\Delta t'}{\Delta t''}} \tag{13}$$

The narrowest flow area f (m^2) between two close tubes is as follows:

$$f = L(S_1 - d) \tag{14}$$

Tube bundle windward surface area F (m^2):

$$F = X \times f \tag{15}$$

The tube bundle heat transfer area A (m^2) is as follows:

$$A = \pi d L n \tag{16}$$

The overall HTC was calculated according to Equation (4).

The HTC between the primary air and wall surface h_1 is calculated via Equations (17)–(20).

Maximum flow velocity u_1 (m/s):

$$u_1 = \frac{Q_1}{F} \tag{17}$$

Reynolds number Re_1:

$$Re_1 = \frac{u_1 d}{\nu_1} \tag{18}$$

When the tube arrangements are staggered arrangements, $0.7 < P_{r1} < 500$, Re_1 = 103~2×10^5, and $S_1/S_2 \leq 2$, the average surface HTC of the tube bundle criterion correlation formula selection [29] is:

$$Nu_1 = 0.31 Re_1^{0.6} \left(\frac{S_1}{S_2}\right)^{0.2} \varepsilon_Z \tag{19}$$

ε_Z, a correction coefficient based on flow pattern, pipeline geometry, or flow conditions, adjusts the model to respond to various flow scenarios.

The convective HTC h_1 is as follows:

$$h_1 = Nu_1 \frac{\lambda}{d} \tag{20}$$

Finally, the values are substituted into Equation (4) to calculate the HTC of wet sides h_2:

$$h_2 = \frac{1}{\frac{1}{K_{eq}} - \frac{1}{h_1} - \frac{\delta_1}{\lambda_1}} \tag{21}$$

The performance of the IEC system can be evaluated in terms of wet-bulb efficiency, which is calculated as [16]:

$$\eta = \frac{t_{g1} - t'_{g2}}{t_{g1} - t_{s2}} \tag{22}$$

2.2. Experimental Procedure

The VTIEC is primarily made up of a vertical-type heat exchanger core, primary and secondary fans, a circulating water pump, and a circulating water tank. The outdoor temperature ranged from 26.6 to 44.9 °C, with a humidity range of 23.4–63.6% during the experiment. A vertical tube indirect evaporative cooler test bench was constructed with a 1.5 m tube length, a 10 mm diameter, and horizontal and vertical spacing of 35 mm and 30 mm, respectively. Figure 4 shows a snapshot of the test rig. Figure 5 shows the schematic diagram for this system. The air opening measures 1.52 m × 1.46 m, while the wetted surface is 1.7 m × 0.85 m.

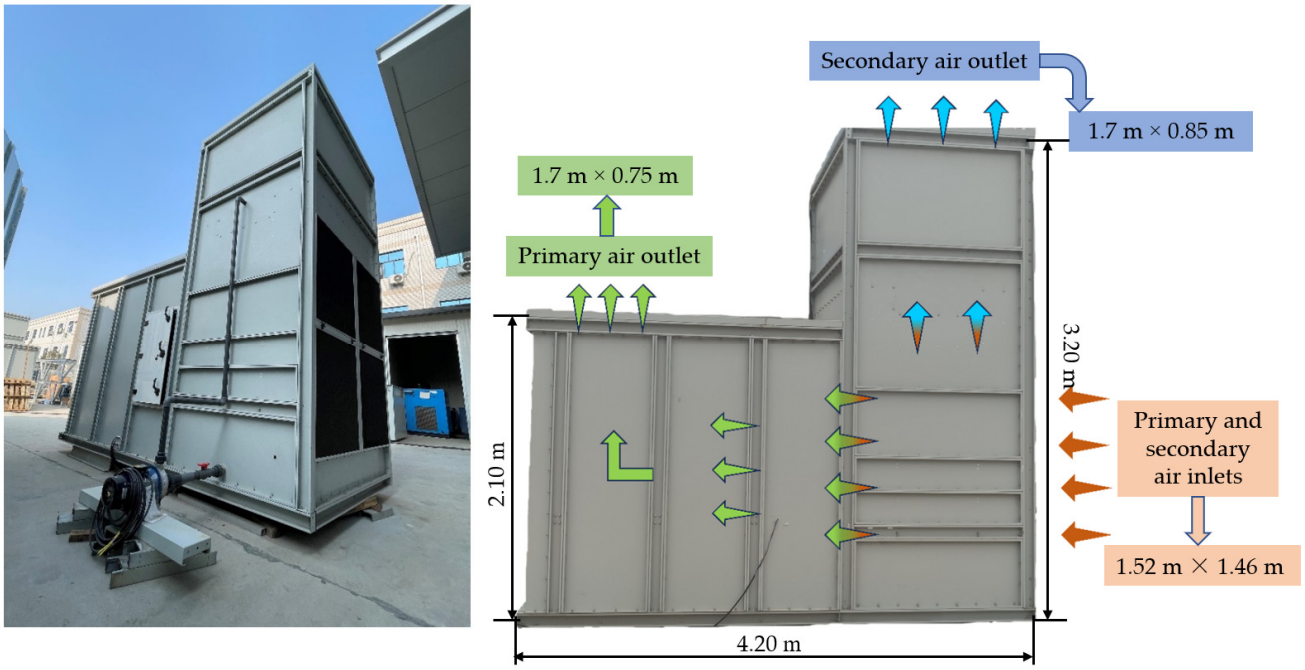


Figure 4. Photo of the test rig.

Temperatures and humidity were monitored using measurement sites at the primary and secondary air exits (points A and B). Additional points were installed in shaded outdoor regions to monitor the unit's inlet air parameters, specifically the outdoor air temperature and humidity. To measure the temperature of the secondary air outflow, thermocouples were inserted above the filler (point C). Measurement sites were also placed in the circulating water tank and heat exchanger core to record the temperatures of the wetted water and the water film inside the pipe. Figure 6 depicts the arrangement of temperature measuring locations on the water film. The thermocouple measurement points 1, 2, and 3 are positioned as shown in the schematic diagram.

In Xi'an, China, where the air is dry and the relative humidity is low, evaporative cooling works especially well in Northwest China's arid regions. Water readily evaporates when in contact with air, absorbing heat and offering a natural, energy-efficient cooling source. Therefore, the use of the wetted water flow rate, primary air volume, and secondary

air volume was adjusted and tested at various outdoor dry bulb temperatures. The water flow rate was set to 2 m^3/h, 3 m^3/h, 4 m^3/h, 5 m^3/h, and 6 m^3/h, and the data for each water flow rate were measured at secondary/primary airflow ratios (AFRs) of 0.3, 0.4, 0.5, 0.6, and 0.7. A total of 25 sets of test circumstances were utilized. Temperature and humidity are measured at 1 min intervals. Table 1 shows the experiment's parameters and the instruments used.

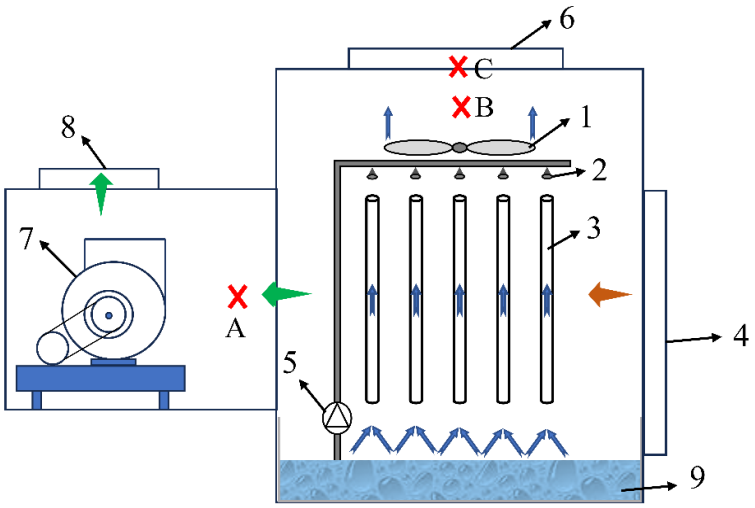


Figure 5. Schematic diagram of the experimental setup. 1. Secondary fan; 2. Nozzle; 3. Heat exchanger core; 4. Air inlets; 5. Circulating water pump; 6. Secondary air outlet; 7. Primary fan; 8. Primary air outlet; 9. Water tank. A, B. Temperature and humidity measurement points; C. Thermocouple measurement points. The legend description was adapted from Sun [12] and Sun [16].

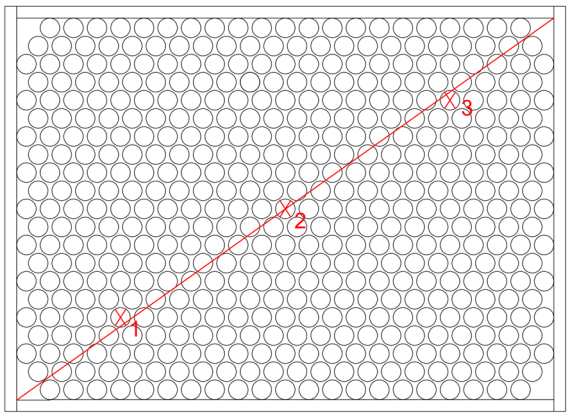


Figure 6. Arrangement of the water film temperature measurement points inside the tubes.

Table 1. Details of the instruments.

Instrument Model	Test Content	Measurement Range	Precision Requirements
Rotronic HL-1D	dry bulb temperature	−30 °C~70 °C	±0.3 °C
Rotronic HL-1D	humidity level	0%RH~100%RH	±3% RH
Testo-480	wind speeds	0 m/s~+50 m/s	±0.1 m/s
pt100	water temperature	−50 °C~200 °C	±0.1 °C
Float Flow Meter	water flow rate	0 m^3/h~12 m^3/h	±0.01 m^3/h
KST-5.0	hourly water temperatures	−200 °C~2400 °C	0.2 FS%
Tape measure	air outlet size	0 m~3 m	1 mm

The h_2 values for wet sides for each situation are calculated using the theory presented in Section 2.1. Table 2 displays the h_2 of wet sides under a selection of test settings.

Table 2. The h_2 of wet sides under a selection of test settings.

Dry Bulb Temperature t_{g1}/°C	Wet Bulb Temperature t_{s1}/°C	Primary Air Temperature $t_{g1'}$/°C	Secondary Air Temperature $t_{g2'}$/°C	Water Flow Rate m^3/h	Secondary/Primary Air Flow Ratio (AFR)	Water Film Temperature t_f/°C	HTC of Wet Sides h_2
26.6	21.91	23.8	23.1	2	0.3	23.7	139.22
25.7	20.67	22.8	21.9	2	0.5	22.8	204.48
28.3	21.07	24.9	21	3	0.7	21.5	34.79
32.9	25.77	29.7	28.5	3	0.3	31.1	180.84
31.8	26.06	28.25	27.8	4	0.7	29	130.04
32.1	25.81	28.75	28.3	4	0.5	29.7	558.6
32.1	25.96	28.6	27.6	4	0.6	30.1	924.5
25.0	20.33	22.2	21.6	5	0.7	21.8	248.7
26.8	21.15	23.7	22.9	6	0.6	23.2	136.8

2.3. Uncertainty Analysis

Uncertainty analysis is an important component of experimental research that evaluates the dependability and correctness of results. This study used Moffat's [30] (1985) uncertainty analysis method to calculate the uncertainties of each parameter. These studies support the dependability of the experimental results. Table 3 displays the findings of the uncertainty analysis.

$$Y = f(x_1, x_2, x_3, \ldots x_n) \tag{23}$$

$$\delta Y = \sqrt{\left(\frac{\partial Y}{\partial x_1}\delta x_1\right)^2 + \left(\frac{\partial Y}{\partial x_2}\delta x_2\right)^2 + \left(\frac{\partial Y}{\partial x_3}\delta x_3\right)^2 + \ldots + \left(\frac{\partial Y}{\partial x_n}\delta x_n\right)^2} \tag{24}$$

Table 3. Uncertainties of various parameters.

Parameter	Uncertainty (%)
temperature	1.9
relative humidity	4.0
wind speed	2.3
wet-bulb efficiency	10.49
HTC of wet sides	3.79

3. Results and Discussion

For a VTIEC system, a greater h_2 on the wet sides suggests a higher overall HTC and better heat transmission. Several parameters influence wet-side h_2. Given the heat transfer scenario on the wet side, the impact of a single element on HTC is rather minor. This study examines how four parameters affect the wet-side h_2 of a VTIEC: outdoor air dry-bulb/wet-bulb temperature difference, air–water ratio, secondary/primary airflow ratio (AFR), and water flow rate. Experiments show that modifying operating parameters in actual applications can produce a wet-side h_2 of 350 W/(m^2·°C), which is regarded as outstanding. Despite measurement and model errors (HTC ± 3.79%, wet-bulb efficiency ± 10.49%), the patterns across water flow rates and AFR conditions are still noteworthy. The ideal working range is 4–5 m^3/h water flow rate, 2.07–3.46 m^3/(m^2·h) spray density, and AFR ≈ 0.5–1.2. This allows for optimal wet-side heat transfer performance and tolerable error influence.

3.1. Effects of the Outdoor Dry-Bulb/Wet-Bulb Temperature Differences

The performance of evaporative cooling is greatly reliant on the ambient dry and wet bulb temperatures. The "Wet Bulb Depression" of the outdoor air indicates air humidity and

cooling potential. A larger dry-bulb temperature difference (ΔT_{db}) directly enhances the driving force of sensible heat transfer, while a larger wet-bulb temperature difference (ΔT_{wb}) significantly increases the evaporation rate and the corresponding latent heat transfer intensity by increasing the vapor partial pressure gradient at the air–water interface. The coupled effect of these two factors maximizes the combined driving force of the enthalpy difference, thereby simultaneously improving cooling capacity and heat transfer coefficient. This effect is particularly significant in dry climates. Larger dry-bulb/wet-bulb temperature variations usually increase the cooling capacity of the equipment and directly affect the wet-bulb efficiency of IEC units.

To completely measure system performance, wet-bulb efficiency is adopted as a crucial criterion. Figure 7 depicts the correlations between wet-side h_2, wet-bulb efficiency, and the dry-bulb/wet-bulb temperature difference in outside air with varying water flow rates and AFR. The red lines, which are similar in appearance to the blue ones, highlight changes in wet-bulb efficiency at the same AFR.

Figure 7e shows that when the unit water flow rate is 6 m^3/h and the spray density is 4.15 $m^3/(m^2 \cdot h)$, the wet-side heat transfer coefficient (h_2) decreases with increasing outdoor air dry-bulb temperature difference at air flow rate ratios (AFRs) of 0.3, 0.6, and 0.7, and the wet-bulb efficiency also decreases. However, when the AFRs are 0.4 and 0.5, both h_2 and wet-bulb efficiency increase with increasing dry-bulb temperature difference, exhibiting a positive correlation consistent with the overall trend, with h_2 reaching its maximum value at AFR = 0.5. Considering the ±3.79% measurement uncertainty of the wet-side heat transfer coefficient listed in Table 3, the actual range of h_2, approximately 350 $W/(m^2 \cdot °C)$, is 337–363 $W/(m^2 \cdot °C)$. Therefore, the above trend remains statistically significant within the error range. A plausible explanation is that excessive spray density causes droplets to rapidly mix and agglomerate on the pipe surface, resulting in a thick and continuous liquid layer or a narrow water column. This results in heat transfer across a thicker liquid phase layer, increasing thermal resistance inside the liquid film and decreasing evaporation rate per unit area [31,32]. At the same time, greater airflow disturbance can cause near-wall flow separation and the formation of a wake region, restricting gas–liquid heat transfer at specific locations and lowering the local heat transfer coefficient. In addition, the Marangoni effect (i.e., the difference in thermal surface tension) drives interfacial flow under the temperature gradient, resulting in fluctuations in liquid film thickness; capillary forces also play an important role in the contraction and rupture of the liquid film [33]. Both of these factors can lead to unstable liquid film and uneven coverage, forming dry spots or fine stream structures, thereby reducing the effective heat transfer area [34]. This reduces the effective h_2 by approximately 5% to 10%. The corresponding wet-bulb efficiency uncertainty can reach ±10.49%, explaining why system performance improvement tends to saturate or even slightly decrease in the high-flow range.

When the water flow rate is between 2 and 5 m^3/h, the wet-side thermal coefficient generally increases with the increase in the outdoor dry-bulb temperature difference. For a water flow rate of 5 m^3/h and a spray density of 3.46 $m^3/(m^2 \cdot h)$, the relative standard deviation of the measured HTC is approximately ±3.79%, indicating that the data fluctuation within this range is well controlled by experimental uncertainty. Even after accounting for the coupled effects of temperature measurement error (±1.9%) and wind speed error (±2.3%), the corrected h_2 increase trend still holds. Therefore, in practical applications, appropriately increasing the water flow rate and utilizing air with a larger dry-bulb temperature difference can significantly improve heat exchange efficiency. To ensure stable thermal performance and a cumulative error of no more than 5%, it is recommended that the water spray density *qw* be controlled within the range of 2.07–3.46 $m^3/(m^2 \cdot h)$.

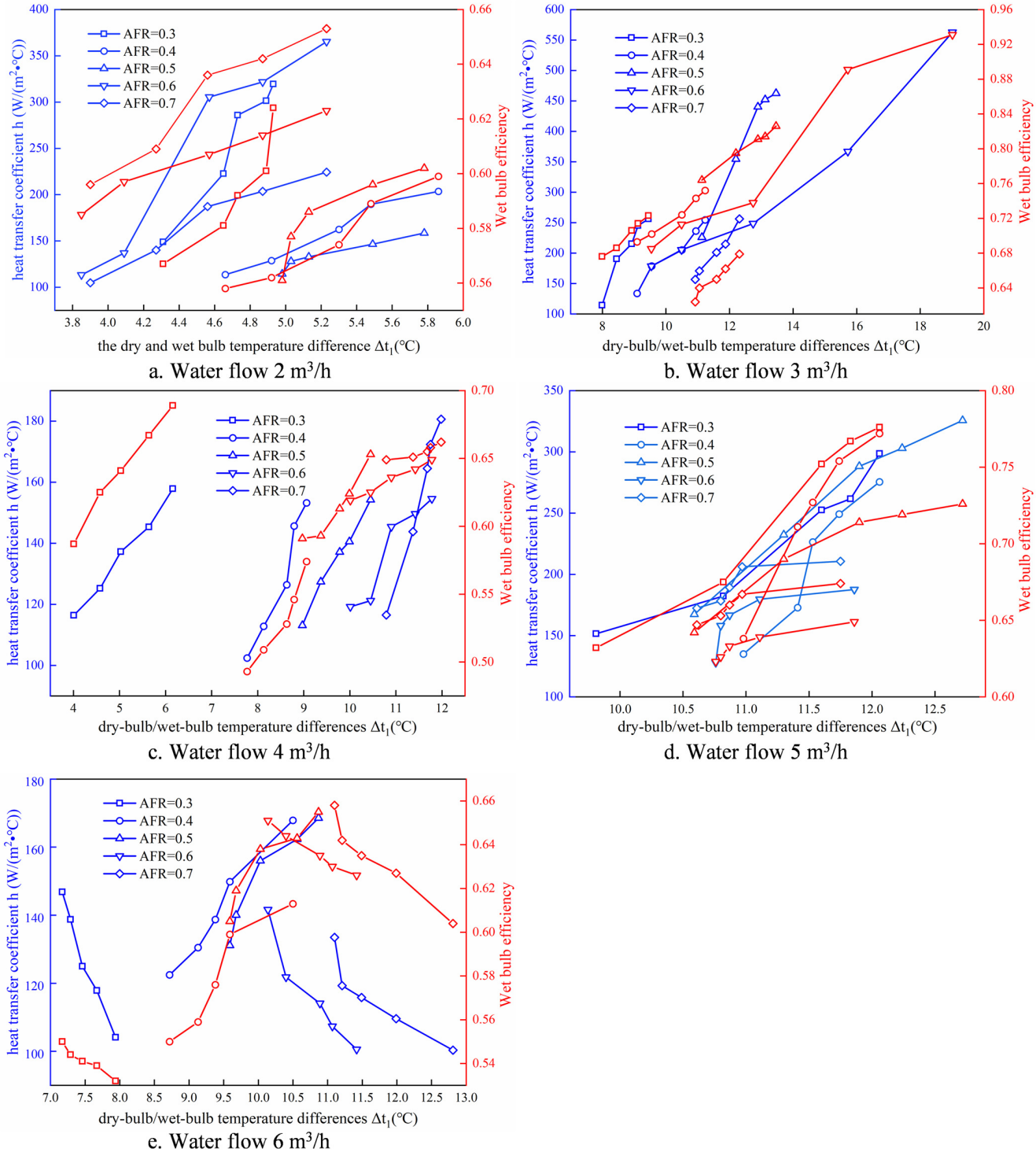


Figure 7. Relationships among the outdoor dry-bulb/wet-bulb temperature difference, the wet-sides h_2, and the efficiency at different water flow rates.

In practical applications, raising the water flow rate and using air with a greater dry-bulb/wet-bulb temperature differential can help to improve heat exchange efficiency. To achieve optimal heat exchange performance, heat exchangers should be designed with diverse operating conditions in mind, as well as appropriate water flow rates and airflow ratios. Based on Figure 7, it is recommended to keep the unit's spray water density qw between 2.07 and 3.46 $m^3/(m^2 \cdot h)$ to avoid inefficiency owing to incorrect AFR. When used in areas with considerable dry-bulb/wet-bulb temperature differential in the external air, the device performs better in heat exchange.

3.2. Effect of the Air-Water Ratio

The air-to-water ratio is a crucial factor in assessing cooling tower efficiency and VTIEC effectiveness. In dry environments (low wet-bulb temperatures), a higher air-to-water ratio can achieve effective cooling; in humid environments (high wet-bulb temperatures), the air-to-water ratio must be lowered to ensure sufficient evaporation and avoid performance degradation. Therefore, the secondary air volume and water flow rate directly impact heat and mass transfer on wet surfaces, which can be influenced by the air–water ratio (n) as shown below.

$$n = \frac{m}{W} \tag{25}$$

Figure 8 shows the coupled relationship between the air-to-water ratio, wet-side heat transfer coefficient (h_2), and wet-bulb efficiency at different water flow rates. As the air-to-water ratio increases, the h_2 decreases; a high water flow rate combined with a low air-to-water ratio can maintain a constant h_2. Considering a measurement uncertainty of ±3.79%, the measured h_2 of 350 W/(m^2·°C) corresponds to a true range of approximately 337–363 W/(m^2·°C). When the water flow rate exceeds 4 m^3/h and the water spray density exceeds 2.77 m^3/(m^2·h), the air-to-water ratio should be controlled below 1.2 to maintain optimal h_2(The best performance data from this investigation correlate to the experimental circumstances mentioned in this article). If the water flow rate is 3 m^3/h, achieving an equivalent h_2 of ≈ 350 W/(m^2·°C) requires increasing the air-to-water ratio by approximately 2.5 times. Considering the instability of the airflow and wet film, the h_2 fluctuation range may increase to ±5%, but the overall trend remains significant. The VTEC investigated in this study consists of two heat exchange cores, each made of a bundle of 469 tubes with a diameter of 10 mm, and has external dimensions of 846 mm × 660 mm × 1460 mm. The studies were conducted under outdoor temperature conditions of 26.6–44.9 °C and relative humidity of 23.4–63.6%. The resulting "optimal steam-to-water ratio" matches the precise operating circumstances indicated above. If the test conditions change, the steam-to-water ratio is no longer guaranteed to be ideal.

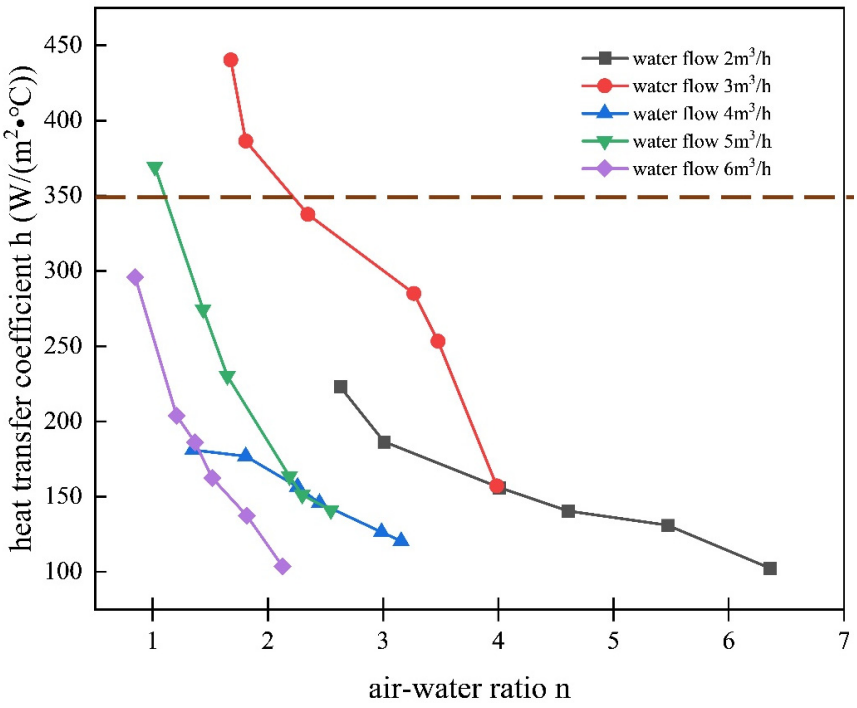


Figure 8. Relationships among the air-water ratio, h_2 of wet sides, and efficiency.

3.3. Effects of the Secondary/Primary Airflow Ratio and Water Flow Rate

In evaporative cooling, the secondary/primary airflow ratio (AFR) is important because differing airflow ratios have a substantial impact on heat transfer efficiency. The ideal airflow ratio is system-specific, and for VTIECs, maintaining an airflow ratio between 0.3 and 0.7 leads to increased unit performance [35].

The wet channel, which uses direct evaporative cooling via the interaction of drench water and secondary air, is especially sensitive to the drench water flow rate, which affects heat exchange efficiency and total cooling performance. As a result, raising the water flow rate typically improves the coefficient of performance of IEC systems. Furthermore, fluctuations in the water flow rate might influence the total water temperature inside the IEC system, highlighting the need to integrate the water flow rate with other parameters to completely examine the impact of wet sides on the h_2.

Figure 9 further demonstrates the interaction between h_2, wet-bulb efficiency, and AFR at different water flow rates when the dry-bulb temperature difference is 8 °C. For a fixed water flow rate, increasing AFR helps improve wet-bulb efficiency. When the water flow rate exceeds 4 m^3/h and the AFR is >0.5, the h_2 approaches 350 $W/(m^2 \cdot °C)$, and the actual range after error correction is approximately 337–363 $W/(m^2 \cdot °C)$. Even considering the combined effect of temperature and humidity measurement errors (approximately 4.5%), this trend remains within the confidence interval. Further analysis shows that, for a fixed AFR, h_2 increases monotonically with increasing water flow rate from 2 to 5 m^3/h. However, heat transfer deteriorates at 6 m^3/h due to shear disturbance and membrane rupture. Combined with uncertainty analysis, the maximum h_2 corresponding to a water flow rate of 5 m^3/h falls within the range of 350 ± 13 $W/(m^2 \cdot °C)$, indicating optimal performance and good repeatability under this operating condition.

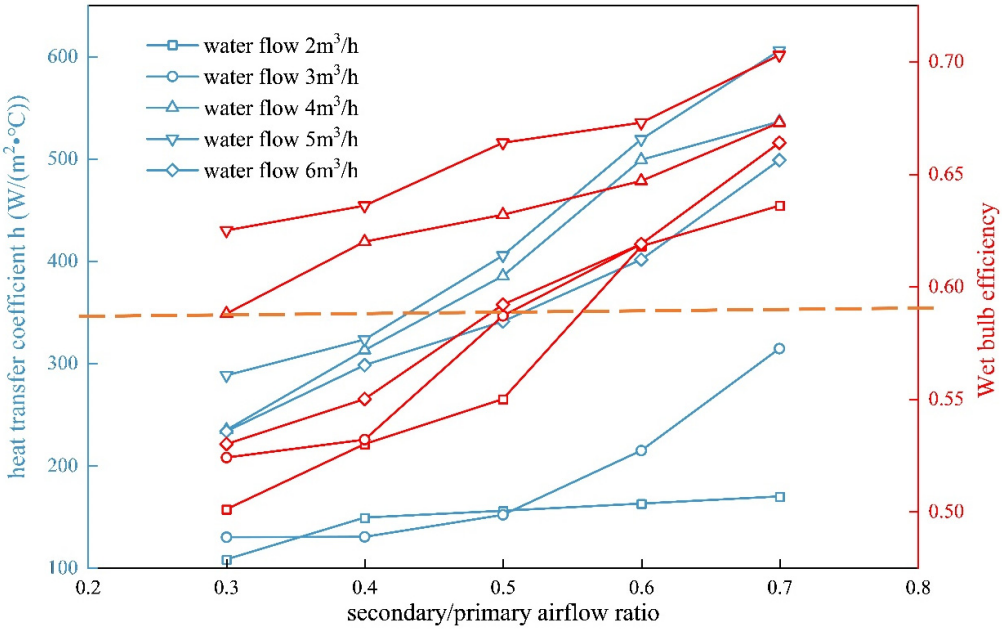


Figure 9. Relationships among the secondary/primary airflow ratio, the h_2 of wet sides, and the wet bulb efficiency.

4. Conclusions

The heat transfer coefficient (h_2) of the wet side of a vertical tube indirect evaporative cooling (VTIEC) system is an important parameter that has a significant impact on the overall performance of the system. However, due to the complexity of the heat and mass transfer processes on the wet side, it is still difficult to accurately predict h_2. This study

investigates the effects of four key parameters on the wet side h_2 of a VTIEC system: outdoor air dry-bulb/wet-bulb temperature difference, air-to-water ratio, secondary/primary air flow ratio (AFR), and water flow rate. The main findings are as follows:

(1) The heat transfer coefficient (h_2) generally increases with the increase in outdoor dry-bulb/wet-bulb temperature difference. However, excessive water flow rate and unbalanced air volume ratio may reduce the heat exchange efficiency. For optimal performance, the water spray density (q_w) should be maintained between 2.07 and 3.46 $m^3/(m^2 \cdot h)$. In addition, installing the unit at a location with a larger dry-bulb/wet-bulb temperature difference can achieve better heat exchange effects.

(2) As the air-to-water ratio increases, the h_2 decreases with increasing water flow rate. The larger the water flow rate, the lower the air–water ratio required to achieve the same h_2. For wet side h_2 exceeding 350 $W/(m^2 \cdot °C)$, the water injection density should exceed 2.07 $m^3/(m^2 \cdot h)$, and the air–water ratio should be less than 2.5. A water flow rate greater than 3 m^3/h is recommended.

(3) Although the experimental verification in this study is mainly for the VTIEC system, the proposed analytical framework and generalized correlations may be applicable to a wider range of IEC system configurations and can be used as future research directions.

In order to optimize the wet-side thermal cycle coefficient of the VTIEC unit, the water injection density should be maintained between 2.07 and 3.46 $m^3/(m^2 \cdot h)$ and the air–fuel ratio (AFR) should be set between 0.5 and 0.6 to ensure that the primary air temperature drop exceeds 6 °C. The system should be deployed in low-humidity areas. These findings provide useful theoretical guidance for engineering applications. Furthermore, considering experimental uncertainties such as variations in film thickness due to uneven water distribution (approximately ±5–10%), temperature measurement deviations due to unstable airflow (approximately ±0.3 °C), and errors in the estimated effective heat transfer area (approximately ±6%), the overall uncertainty of the wet-side h_2 calculated in this study is approximately ±8–12%. Therefore, further efforts are needed to reduce parameter measurement errors and improve the reliability and applicability of the model.

Author Contributions: Conceptualization, T.S. and P.L.; Funding acquisition, T.S.; formal analysis, G.T. and H.S.; Investigation, W.L.; Methodology, W.L.; Visualization, H.S.; Writing—original draft, P.L. All authors have read and agreed to the published version of the manuscript.

Funding: This work was supported by the Natural Science Basic Research Program of Shaanxi (2025JC-YBMS-510); Key Research and Development Projects of Shaanxi Province (2025JH-ZDLJQ-0005).

Data Availability Statement: The data that support the findings of this study are openly available in figshare at https://doi.org/10.6084/m9.figshare.28547189.v1.

Conflicts of Interest: The authors declare that the research was conducted in the absence of any commercial or financial relationships that could be construed as a potential conflict of interest.

Nomenclature

A heat exchanger area (m^2);
C_p specific heat capacity at constant pressure ($kJ/(kg \cdot °C)$);
d equivalent diameter (m);
f the narrowest flow area between two neighboring tubes (m^2);
F total circulation area (m^2);
h heat transfer coefficient ($W/(m^2 \cdot °C)$);
i_f enthalpy value of saturated air at the water film surface (kJ/kg);
i_{g1} enthalpy value at the primary air inlet (kJ/kg);
$i_{g1'}$ enthalpy value at the primary air outlet (kJ/kg);

K_{eq}	overall heat transfer coefficient (W/(m^2·°C));
L	length of the tube (m);
m	mass flow rate (kg/s);
N	the number of total vertical tubes;
Nu	Nusselt number, $Nu = \frac{h \cdot d}{\lambda}$;
Pr	Prandtl number, $Pr = \frac{\nu}{\alpha}$;
Q	Volumetric flow rate (m^3/h);
q_w	water spraying density (m^3/(m^2·h);
Re	Reynolds number, $Re = \frac{u \cdot d}{\nu}$;
S_1	lateral pipe spacing (m);
S_2	longitudinal pipe spacing (m);
S_w	water spraying area (m^2);
t_f	water film temperature (°C);
t_{g1}	primary air inlet dry bulb temperature (°C);
$t_{g1'}$	primary air outlet dry bulb temperature (°C);
t_{g2}	secondary air inlet dry bulb temperature (°C);
$t_{g2'}$	secondary air outlet dry bulb temperature (°C);
t_s	wet bulb temperature (°C);
T_W	tube wall temperature (°C);
u	airflow velocity (m/s);
X	number of tubes on the windward side.

Greek Symbols

α	thermal diffusivity, (m^2/s);
δ	thickness of heat conduction medium (m);
Δi_m	log mean enthalpy difference (kJ/kg);
Δt_m	log mean temperature difference (°C);
ΔT_{db}	dry-bulb temperature difference;
ΔT_{wb}	wet-bulb temperature difference;
ε_Z	tube bank correction factor;
λ	thermal conductivity (W/(m·°C));
ν	fluid motion viscosity coefficient (m^2/s);
ρ	density (kg/m^3);
Φ	Overall Heat transfer quantity (W);
φ	relative humidity (%RH).

Abbreviations

AFR	secondary/primary airflow ratio;
CFD	Computational fluid dynamics;
DEC	Direct evaporative cooler;
HTC	Heat transfer coefficient;
IEC	Indirect evaporative cooler;
LMTD	Logarithmic mean temperature difference;
VTIEC	Vertical tube indirect evaporative cooler.

References

1. Jamil, M.A.; Shahzad, M.W.; Xu, B.B.; Imran, M.; Ng, K.C.; Zubair, S.M.; Markides, C.N.; Worek, W.M. Energy-efficient indirect evaporative cooler design framework: An experimental and numerical study. *Energy Convers. Manag.* **2023**, *292*, 117377. [CrossRef]
2. Laknizi, A.; Mahdaoui, M.; Abdellah, A.B.; Anoune, K.; Bakhouya, M.; Ezbakhe, H. Performance analysis and optimal parameters of a direct evaporative pad cooling system under the climate conditions of Morocco. *Case Stud. Therm. Eng.* **2019**, *13*, 100362. [CrossRef]

3. Jain, J.K.; Hindoliya, D.A. Experimental performance of new evaporative cooling pad materials. *Sustain. Cities Soc.* **2011**, *1*, 252–256. [CrossRef]
4. Bruno, F. On-site experimental testing of a novel dew point evaporative cooler. *Energy Build.* **2011**, *43*, 3475–3483. [CrossRef]
5. Yang, Y.; Cui, G.; Lan, C.Q. Developments in evaporative cooling and enhanced evaporative cooling—A review. *Renew. Sustain. Energy Rev.* **2019**, *113*, 109230. [CrossRef]
6. Sajjad, U.; Abbas, N.; Hamid, K.; Abbas, S.; Hussain, I.; Ammar, S.M.; Sultan, M.; Ali, H.M.; Hussain, M.; Rehman, T.-U.; et al. A review of recent advances in indirect evaporative cooling technology. *Int. Commun. Heat Mass Transf.* **2021**, *122*, 105140. [CrossRef]
7. Kashyap, S.; Sarkar, J.; Kumar, A. Proposal and month-wise performance evaluation of a novel dual-mode evaporative cooler. *Heat Mass Transf.* **2019**, *55*, 3523–3536. [CrossRef]
8. Duan, Z.; Zhan, C.; Zhang, X.; Mustafa, M.; Zhao, X.; Alimohammadisagvand, B.; Hasan, A. Indirect evaporative cooling: Past, present and future potentials. *Renew. Sustain. Energy Rev.* **2012**, *16*, 6823–6850. [CrossRef]
9. Chang, J.; Huang, X.; Jia, C.; Du, D.; Xu, J. Design and Applicability Study of Vertical Tube Indirect Evaporative Cooler. *Liuti Jixie* **2020**, *48*, 68–73.
10. Pandelidis, D.; Cichoń, A.; Pacak, A.; Drąg, P.; Drąg, M.; Worek, W.; Cetin, S. Water desalination through the dewpoint evaporative system. *Energy Convers. Manag.* **2021**, *229*, 113757. [CrossRef]
11. Cui, X.; Yang, C.; Yan, W.; Zhang, L.; Wan, Y.; Chua, K.J. Experimental study on a moisture-conducting fiber-assisted tubular indirect evaporative cooler. *Energy* **2023**, *278*, 128014. [CrossRef]
12. Sun, T.; Tang, T.; Yang, C.; Yan, W.; Cui, X.; Chu, J. Cooling performance and optimization of a tubular indirect evaporative cooler based on response surface methodology. *Energy Build.* **2023**, *285*, 112880. [CrossRef]
13. Sun, T.; Tang, T.; Ma, J.; Yan, Y.; Fu, T.; Zhang, H.; Li, J.; Li, W.; Shen, H.; Huan, C. Experimental study on the flow resistance of inner tube and characteristics of drifting water in a tubular indirect evaporative cooler. *Int. J. Refrig.* **2024**, *160*, 275–297. [CrossRef]
14. Sohani, A.; Sayyaadi, H. Thermal comfort based resources consumption and economic analysis of a two-stage direct-indirect evaporative cooler with diverse water to electricity tariff conditions. *Energy Convers. Manag.* **2018**, *172*, 248–264. [CrossRef]
15. Sun, T.; Huang, X.; Qu, Y.; Wang, F.; Chen, Y. Theoretical and Experimental study on Heat and Mass Transfer of A Porous Ceramic Tube Type Indirect Evaporative Cooler. *Appl. Therm. Eng.* **2020**, *173*, 115211. [CrossRef]
16. Sun, T.; Sun, H.; Tang, T.; Yan, Y.; Li, P. Experimental Study on the Thermal Performances of a Tube-Type Indirect Evaporative Cooler. *Fluid Dyn. Mater. Process.* **2023**, *19*, 2519–2531. [CrossRef]
17. Yuan, F.; Chen, Q. Optimization criteria for the performance of heat and mass transfer in indirect evaporative cooling systems. *Chin. Sci. Bull.* **2012**, *57*, 687–693. [CrossRef]
18. Hasan, A. Going below the wet-bulb temperature by indirect evaporative cooling: Analysis using a modified ε-NTU method. *Appl. Energy* **2012**, *89*, 237–245. [CrossRef]
19. Rajski, K.; Danielewicz, J.; Brychcy, E. Performance Evaluation of a Gravity-Assisted Heat Pipe-Based Indirect Evaporative Cooler. *Energies* **2020**, *13*, 200. [CrossRef]
20. Wan, Y.; Soh, A.; Shao, Y.; Cui, X.; Tang, Y.; Chua, K.J. Numerical study and correlations for heat and mass transfer coefficients in indirect evaporative coolers with condensation based on orthogonal test and CFD approach. *Int. J. Heat Mass Transf.* **2020**, *153*, 119580. [CrossRef]
21. Lin, J.; Bui, D.T.; Wang, R.; Chua, K.J. On the fundamental heat and mass transfer analysis of the counter-flow dew point evaporative cooler. *Appl. Energy* **2018**, *217*, 126–142. [CrossRef]
22. Yang, H.; Shi, W.; Chen, Y.; Min, Y. Research development of indirect evaporative cooling technology: An updated review. *Renew. Sustain. Energy Rev.* **2021**, *145*, 111082. [CrossRef]
23. Kabeel, A.E.; Bassuoni, M.M.; Abdelgaied, M. Experimental study of a novel integrated system of indirect evaporative cooler with internal baffles and evaporative condenser. *Energy Convers. Manag.* **2017**, *138*, 518–525. [CrossRef]
24. Caruana, R.; De Antonellis, S.; Marocco, L.; Guilizzoni, M. Modeling of Indirect Evaporative Cooling Systems: A Review. *Fluids* **2023**, *8*, 303. [CrossRef]
25. Huang, L.; Aute, V.; Radermacher, R. Uncertainty Analysis on Prediction of Heat Transfer Coefficient and Pressure Drop in Heat Exchangers Due to Refrigerant Property Prediction Error. In Proceedings of the International Refrigeration and Air Conditioning Conference, West Lafayette, IN, USA, 14–17 July 2014.
26. Zhang, T.; Su, M.; Zhang, H.; Liu, C.; Ouyang, X. Design and simulation of a new type of fin-and-tube heat exchanger with trapezoidal slit fins. *Case Stud. Therm. Eng.* **2024**, *59*, 104604. [CrossRef]
27. Zeng, T. Research on Air Conditioning System Driven by Low-Concentration Solution Dehumidification Heat Pump. Master's Thesis, Southeast University, Nanjing, China, 2017.
28. Cao, Y. Equivalent Enthalpy Model and Log-Mean Enthalpy Difference Method for Heat-Mass Transfer in Cooling Towers. *ASME J. Heat Mass Transf.* **2024**, *146*, 104501. [CrossRef]
29. Zhang, X. *Heat Transfer Science*, 6th ed.; China Building Industry Press: Beijing, China, 2014.
30. Moffat, R.J. Using Uncertainty Analysis in the Planning of an Experiment. *J. Fluids Eng.* **1985**, *107*, 173–178. [CrossRef]

31. Zhao, H.; Poole, R.; Zhou, Z. Rate-limiting factors in thin-film evaporative heat transfer processes. *Int. J. Heat Mass Transf.* **2024**, *228*, 125629. [CrossRef]
32. Zhang, X.; Zhu, X.; Qiu, Q. Study on liquid film thickness and flow characteristics of falling film outside an elliptical tube. *Desalination Water Treat.* **2019**, *157*, 1–7. [CrossRef]
33. Lim, E.; Hung, Y.M. Thermocapillary flow in evaporating thin liquid films with long-wave evolution model. *Int. J. Heat Mass Transf.* **2014**, *73*, 849–858. [CrossRef]
34. Hajal, J.E.; Thome, J.R.; Cavallini, A. Condensation in horizontal tubes, part 1: Two-phase flow pattern map. *Int. J. Heat Mass Transf.* **2003**, *46*, 3349–3363. [CrossRef]
35. Song, X.; Huang, X.; Li, X.; Zhang, L.; Qiu, J. A preliminary study on the experiment of vertical tube indirect evaporative cooler. *J. Build. Heat Vent. Air Cond.* **2015**, *34*, 52–55.

Disclaimer/Publisher's Note: The statements, opinions and data contained in all publications are solely those of the individual author(s) and contributor(s) and not of MDPI and/or the editor(s). MDPI and/or the editor(s) disclaim responsibility for any injury to people or property resulting from any ideas, methods, instructions or products referred to in the content.